A Synthesis-free Directional Modulation Transmitter using Retrodirective Array

Ding, Y., & Fusco, V. (2016). A Synthesis-free Directional Modulation Transmitter using Retrodirective Array. IEEE Journal of Selected Topics in Signal Processing. DOI: 10.1109/JSTSP.2016.2605066

Published in:
IEEE Journal of Selected Topics in Signal Processing

Document Version:
Peer reviewed version

A Synthesis-free Directional Modulation Transmitter using Retrodirective Array

Yuan Ding, and Vincent Fusco, *Fellow, IEEE*

***Abstract*—By modification of the classical retrodirective arrays (RDAs) architecture a directional modulation (DM) transmitter can be realized without the need for synthesis. Importantly, through analytical analysis and exemplar simulations, it is proved that, besides the conventional DM application scenario, i.e., secure transmission to one legitimate receiver located along one spatial direction in free space, the proposed synthesis-free DM transmitter should also perform well for systems where there are more than one legitimate receivers positioned along different directions in free space, and where one or more legitimate receivers exist in a multipath environment. None of these have ever been achieved before using synthesis-free DM arrangements.**

***Index Terms*—Directional modulation (DM), information pattern, interference pattern, retrodirective array (RDA), synthesis-free.**

I. Introduction

DIRECTIONAL modulation (DM) is a promising technology, being categorized as a keyless physical-layer wireless security means. It endows transmitters the ability to distort signal waveform signatures projected wirelessly along all spatial directions in free space other than an a-priori selected direction along which a legitimate receiver locates [1].

In some early reported DM work the characteristic of the direction-dependent signal modulation format transmission was achieved by directly reconfiguring the antenna radiating elements during data transmission. Here re-configurability was realized by either altering the near-field electromagnetic boundaries [2], [3], or by re-routing the excitation currents on radiating structures [4], resulting in changeable far-field radiation patterns that were direction-dependent. The major problem associated with these DM architectures is lack of effective synthesis methods because there are no analytical means to describe the complex interaction between the near-field boundaries or current distributions and their far-field radiation behaviors. This problem was solved by introducing excitation-reconfigurable antenna arrays, which have ability to update array excitation weightings on a per transmitted symbol basis. At first the excitation weighting updates were performed using attenuators and phase shifters at radio frequency (RF) frontends [5]–[9], then it was illustrated in [10] that excitation could also be updated in the digital baseband, avoiding the use of more expensive yet less precise RF reconfigurable components.

Synthesis methods for excitation reconfigurable DM transmitter arrays have progressed greatly in recent years. Bit error rate (BER) driven optimization algorithm assisted approaches were presented in [5], [6], [11], [12]. A variety of DM synthesis methods by constraining different properties of array far-field radiation patterns were described in [13]–[17]. An orthogonal vector approach was firstly proposed in [1] and further refined in [18], which synthesizes DM transmitter arrays by generating orthogonal vectors/interference in the null space of the channel vectors between the DM transmitters and the legitimate receivers. This approach is relatively universal as it is compatible with both static and dynamic DM systems [19], and can be readily deployed into modern digital wireless transmitters [20]. Furthermore, the orthogonal vector approach can be readily extented to endow DM transmitters with the ability for multiple independent secure beam transmissions [21]–[23] and to make the DM technology applicable in multipath environment [24], [25]. Using the orthogonal vector concept the DM synthesis can be considered as a process of injecting artificial interference that is orthogonal to the transmitted information signals along selected direction(s) in free space or at desired location(s) within a multipath environment. In other words it is the process of generating far-field patterns, in free space, or far-field distributions, in multipath environments, which have power null(s) at location(s) where intended receiver(s) is/are placed. Since artificial interference is injected into DM systems through these patterns, we shall refer to them as interference patterns hereafter. Similarly the far-field patterns through which information signals are conveyed are labelled as information patterns in this paper. For more detailed information on DM technology, interested readers are suggested to read the overview papers [26], [27].

Some practical issues with all of the above mentioned DM synthesis approaches include the acquisition of the desired secure communication direction along which the legitimate receiver locates, and the demand of heavy computation, especially for dynamic DM systems, as well as applications in the multipath environment. These hinder the real-time response of implemented DM transmitters. For example, the BER-driven methods in [5], [12] and the far-field radiation pattern synthesis approaches in [14], [15] require a number of iterations in optimization processes; the far-field pattern separation method

Yuan Ding, and Vincent Fusco are with the Institute of Electronics, Communications and Information Technology (ECIT), Queen's University of Belfast, Belfast, United Kingdom, BT3 9DT (phone: +44(0)2890971806; fax: +44(0)2890971702; e-mail: yding03@qub.ac.uk; v.fusco@ecit.qub.ac.uk).

[16], [17] and the orthogonal vector approach or the MIMO-inspired approach [1], [21]–[25] involves matrix inversion. In addition when the selected secure communication direction/location or the multipath environment changes all of the DM synthesis processes need to be re-run.

Two recently proposed DM transmitter architectures alleviate the requirement of heavy computation in some application scenarios. They are termed synthesis-free DM transmitters. One achieves DM functionality by activating a random subset of antenna elements for each symbol transmission along the desired direction, to which the entire phased array is beam steered. This concept was named antenna subset modulation (ASM) in [28], [29] or four-dimensional (4-D) arrays in [30], [31]. However, this type of DM transmitters greatly reduces available beam-forming gain, and also, is not applicable for multi-beam secure transmission scenarios and multipath channel environment usage. The other synthesis-free DM structure exploits the beam orthogonality property of the Fourier beam-forming networks to generate the artificial interference that is orthogonal to genuine information signals, i.e., has a far-field power null, along the prescribed secure communication direction [32]–[34]. However, this type of DM arrangment suffers high insertion loss and low spatial pointing resolution, and again it is not suitable for use in multipath environments.

In this paper we propose a new type of DM transmitter which builds upon a classical retrodirective array (RDA). This novel DM solution has a series of advantages that are summarized as below;

1) No extra target direction detection estimation facilities are required since automatic target tracking is the inherent functionality that an RDA possesses. The retrodirection ability can be achieved using low power purely analogue phase conjugation circuitry that enables real-time response, [35], [36];
2) It is DM synthesis-free. The generation of orthogonal interference that is used to achieve DM functionality [1], i.e., signal waveform distortion along all spatial directions other than the secure communication direction, is independent of the selected secure direction, and, importantly, can be performed using low-cost low-complexity analogue solutions for real-time behaviour;
3) The proposed DM architecture can operate in the scenario where multiple legitimate receivers located along different directions in free space acquire the same information that is required to be conveyed securely. This is completely un-related to the 'dual-beam' DM in [37], which utilizes two beams transmitted along the same direction to construct a single-beam DM transmitter, and is also different to the multi-beam DM in [21]–[23], where multiple DM beams for independent information transmissions are formed;
4) The proposed DM architecture can operate in a multipath environment.

It should be noted that the RDA and the DM technologies were previously linked together in [24], [25]. However, unlike the synthesis-free RDA DM architecture proposed in this paper, the orthogonal interference generation in all previous work is direction-dependent, and demands heavy computation.

This paper is organized as follows. In Section II the proposed synthesis-free RDA DM transmitter architecture is described. This is followed by validation under three different application scenarios in Sections III, IV, and V, respectively. For each case both analytical analysis and simulation examples are presented. A brief discussion on its hardware implementation is provided in Section VI. Conclusions on the work are presented in Section VII.

Throughout this paper, the following notations will be used: Boldface capital letter denotes a complex number; Boldface capital letter with an arrow on top represents a vector, whose elements are complex numbers, and whose subscript represents the number of its elements, e.g., $\vec{\boldsymbol{U}}_N = \left[\boldsymbol{U}_1 \quad \boldsymbol{U}_2 \quad \cdots \quad \boldsymbol{U}_N\right]^T$; Capital letter with a bar on top means the complement of the designated set; $(\bullet)^T$ denotes vector transpose operator; '$|\bullet|$' refers to modulus of a complex number; Operator '$\circ$' is the Hadamard product of two vectors; The sign '$\rightarrow$' in the text means 'be convergent to'.

II. Proposed Synthesis-free RDA DM Transmitter

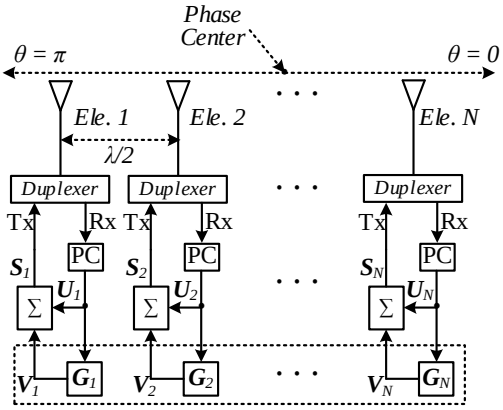

Fig. 1. Proposed synthesis-free RDA DM transmitter architecture.

The proposed synthesis-free RDA DM transmitter architecture comprising N antenna elements is illustrated in Fig. 1. Here for clarity the frequency down-conversion and up-conversion components normally involved in the phase conjugators (PCs) in the receive (Rx) chains and the signal modulation in the re-transmit (Tx) chains are omitted. In the Rx mode the pilot tone signal(s) from legitimate receiver(s) impinged on the antenna array is/are phase conjugated as occurs in classical RDAs. Before up-conversion for re-transmission, the phase conjugated signal vector $\vec{\boldsymbol{U}}_N$ is combined with a vector $\vec{\boldsymbol{V}}_N$, which is derived from $\vec{\boldsymbol{U}}_N$ by weighting a network $\vec{\boldsymbol{G}}_N$. We denote the combined re-transmission signal vector as $\vec{\boldsymbol{S}}_N$, i.e., $\vec{\boldsymbol{S}}_N = \vec{\boldsymbol{U}}_N + \vec{\boldsymbol{V}}_N$. It will be shown in Sections III, IV, and V for different application scenarios that the re-transmitted signal beams are capable of being automatically steered towards the legitimate receiver(s), eliminating additional target direction detection hardware, and the signal waveform signatures transmitted elsewhere are

randomly distorted. More importantly the DM enabling network $\vec{\boldsymbol{G}}_N$ is independent of the direction(s) or position(s) where legitimate receiver(s) locates, i.e., DM is synthesis-free.

In this paper it is assumed that all of the co-frequency pilot tones are radiated only by legitimate receivers. For the case when a malicious third party radiates a co-frequency pilot tone, the RDA re-transmitted information could be 'received' by the third party. This issue can be solved using sub-array concept, using which a power null is formed along the undesired receiver, as described in [38], or using some special-case pilot-tone spectral signatures presented in [39]. Another solution is to use modulated pilot signals within which the identifications of the legitimate receivers can be encoded for authentication purpose at RDA side. It should be pointed out that the PCs can operate with phase modulated pilot signals [40] which could be used for this purpose.

In order to facilitate analysis in the following sections, it is assumed that the RDA DM transmitter considered in this paper consists of a uniformly spaced N-by-1 antenna array with each element having an identical isotropic radiation pattern, $\lambda/2$ separated, where λ refers to the wavelength corresponding to the system's operating frequency.

III. Validation with One Legitimate Receiver in Free Space

When one legitimate receiver is located along the spatial direction α in free space and emits a pilot tone signal, the received pilot tone signal on the n^{th} array element is $e^{j\pi[n-(N+1)/2]\cos\alpha}$. Here $\alpha \in \theta = [0, \pi]$. Throughout we assume that the path loss is normalized out, and the phase reference is chosen as the array's geometric center. Thus the phase conjugated signal vector $\vec{\boldsymbol{U}}_N$ can be written as

$$\vec{\boldsymbol{U}}_N = \left[e^{-j[1-(N+1)/2]\pi\cos\alpha} \quad e^{-j[2-(N+1)/2]\pi\cos\alpha} \quad \cdots \quad e^{-j[N-(N+1)/2]\pi\cos\alpha} \right]^T \tag{1}$$

The re-transmitted radiation pattern $\boldsymbol{P}$ as a function of spatial direction θ, see illustration in Fig. 1, is

$$\boldsymbol{P}(\theta) = \vec{\boldsymbol{S}}_N \cdot \vec{\boldsymbol{F}}_N = \left(\vec{\boldsymbol{U}}_N + \vec{\boldsymbol{V}}_N\right) \cdot \vec{\boldsymbol{F}}_N = \left(\vec{\boldsymbol{U}}_N + \vec{\boldsymbol{G}}_N \circ \vec{\boldsymbol{U}}_N\right) \cdot \vec{\boldsymbol{F}}_N \tag{2}$$

Here $\vec{\boldsymbol{F}}_N$ is the array factor (AF) vector, taking the form in (3),

$$\vec{\boldsymbol{F}}_N = \left[e^{j[1-(N+1)/2]\pi\cos\theta} \quad e^{j[2-(N+1)/2]\pi\cos\theta} \quad \cdots \quad e^{j[N-(N+1)/2]\pi\cos\theta} \right]^T \tag{3}$$

Substituting (1) and (3) into (2), we get

$$\begin{aligned} \boldsymbol{P}(\theta) &= \underbrace{\vec{\boldsymbol{U}}_N \cdot \vec{\boldsymbol{F}}_N}_{\boldsymbol{P}_{info}} + \underbrace{\left(\vec{\boldsymbol{G}}_N \circ \vec{\boldsymbol{U}}_N\right) \cdot \vec{\boldsymbol{F}}_N}_{\boldsymbol{P}_{inter}} \\ &= \underbrace{\sum_{n=1}^{N} e^{j[n-(N+1)/2]\pi(\cos\theta-\cos\alpha)}}_{\boldsymbol{P}_{info}} + \underbrace{\sum_{n=1}^{N} \left\{ \boldsymbol{G}_n e^{j[n-(N+1)/2]\pi(\cos\theta-\cos\alpha)} \right\}}_{\boldsymbol{P}_{inter}} \end{aligned} \tag{4}$$

If we design a network $\vec{\boldsymbol{G}}_N$ wherein

$$\sum_{n=1}^{N} \boldsymbol{G}_n = 0 \tag{5}$$

then re-visiting (4), we can obtain

$$\boldsymbol{P}(\theta)\big|_{\theta=\alpha} = \underbrace{N}_{\boldsymbol{P}_{info}} + \underbrace{\sum_{n=1}^{N} \boldsymbol{G}_n}_{\boldsymbol{P}_{inter}=0} = N \tag{6}$$

which indicates the power projected along direction α is constant, while along other directions $\boldsymbol{P}(\theta)|_{\theta\neq\alpha}$ is dependent on $\vec{\boldsymbol{G}}_N$. $\vec{\boldsymbol{G}}_N$ can be randomly selected as long as (5) is satisfied.

The far-field pattern $\boldsymbol{P}(\theta)$ is separated into the information pattern $\boldsymbol{P}_{info}$, and the interference pattern $\boldsymbol{P}_{inter}$, which is used to distort signal modulation formats along all directions other than the desired secure communication direction α. Fig. 2 shows the calculated power normalized $|\boldsymbol{P}_{info}(\theta)|$ and 10 randomly generated $|\boldsymbol{P}_{inter}(\theta)|$ when, for example, $N = 9$ and $\alpha = 60°$. It is observed that all $|\boldsymbol{P}_{inter}(\theta)|$ patterns have perfect power nulls along the direction α. As a consequence, when the modulated re-transmission signals are superimposed onto the $\boldsymbol{P}(\theta)$, the undistorted signal constellation diagram in IQ space can be detected only along this selected direction α. For illustration purpose, Fig. 3 depicts the far-field radiation patterns for 50 random QPSK symbols transmitted. For each symbol the network $\vec{\boldsymbol{G}}_N$ is arbitrarily selected under the constraints (5) and (7).

$$\sum_{n=1}^{N} \left|1 + \boldsymbol{G}_n\right|^2 = 2N \tag{7}$$

The power efficiency of a DM system, $\mathrm{PE}_{\mathrm{DM}}$, defined in [1], describes the percentage of the total radiated energy that is utilized for useful information transmission. Thus with the condition in (7) the $\mathrm{PE}_{\mathrm{DM}}$ of the example DM system in Fig. 3 is 50%, see (8).

$$\begin{aligned} \mathrm{PE}_{\mathrm{DM}} &= \frac{\int_{\theta=0}^{\theta=\pi} \left|\boldsymbol{P}_{info}\right|^2 d\theta}{\int_{\theta=0}^{\theta=\pi} \left|\boldsymbol{P}_{info} + \boldsymbol{P}_{inter}\right|^2 d\theta} = \frac{\sum_{n=1}^{N} \left|\boldsymbol{U}_n\right|^2}{\sum_{n=1}^{N} \left|\boldsymbol{U}_n + \boldsymbol{G}_n \boldsymbol{U}_n\right|^2} \\ &= \frac{N}{\sum_{n=1}^{N} \left|1 + \boldsymbol{G}_n\right|^2} = \frac{N}{2N} \times 100\% = 50\% \end{aligned} \tag{8}$$

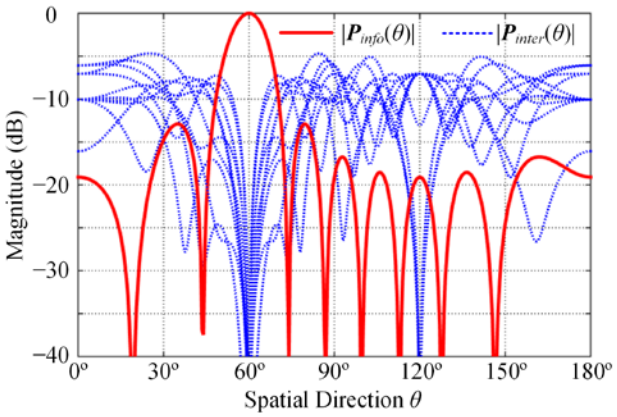

Fig. 2. Simulation example of power normalized information patterns $|P_{info}(\theta)|$ and 10 randomly generated orthogonal interference patterns $|P_{inter}(\theta)|$. N = 9, α = 60°, and PE_{DM} = 50%.

In free space the far-field patterns can be interpreted as constellation patterns in IQ space. Thus from Fig. 3 it can be observed that the standard QPSK constellation diagram, i.e., four symbols with identical amplitude and 90° phase intervals, can be detected only along the selected communication direction, 60° in this example.

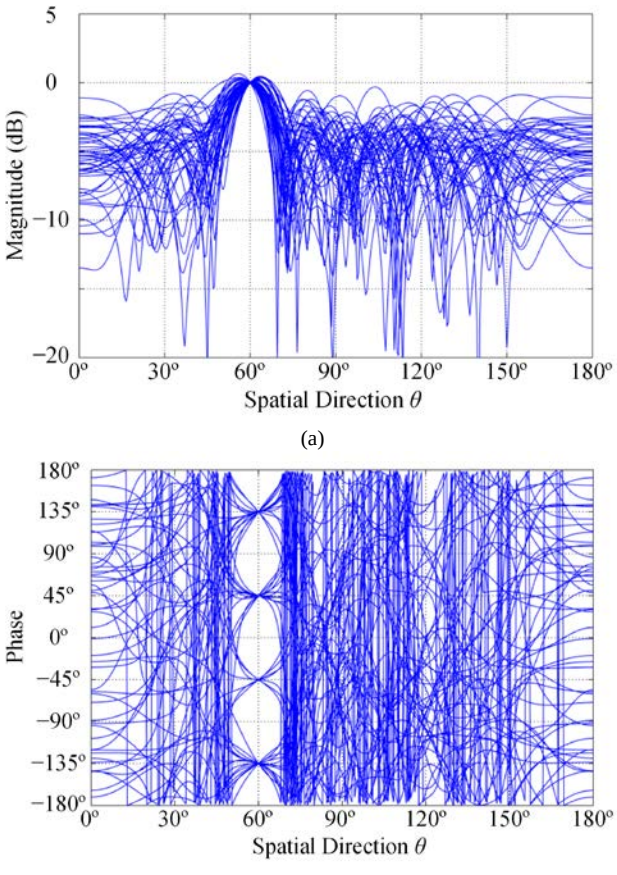

Fig. 3. Simulated far-field (a) magnitude and (b) phase patterns for 50 random QPSK symbols transmitted via the example RDA DM system. N = 9, α = 60°, and PE_{DM} = 50%.

As it has been pointed out previously in [1] and [21] that the achievable secrecy performance is determined by the chosen PE_{DM}, the BER simulation results presented here show the same conclusion, i.e., the smaller PE_{DM} the narrower the BER main beams become and the greater the BER sidelobes are suppressed, as is evident in Fig. 4 under different signal to noise ratios (SNRs). The detailed BER calculation procedures can be found in [19].

IV. Validation with Multiple Legitimate Receivers in Free Space

When multiple devices interrogate a classical RDA using identical frequency pilot tones, the RDA re-transmitted far-field patterns will form multiple main beams in free space whose magnitudes are proportionate to the strengths of the incoming pilot signals [41], [42]. Firstly in this section the scenario of two legitimate receivers located along directions α and β ($\alpha \neq \beta$), respectively, in free space is taken as an example. It is also assumed that the detected signal strengths of two pilot tones from α and β by the RDA DM transmitter are identical. Scenarios with more than two intended receivers in free space are then discussed at the end of this section.

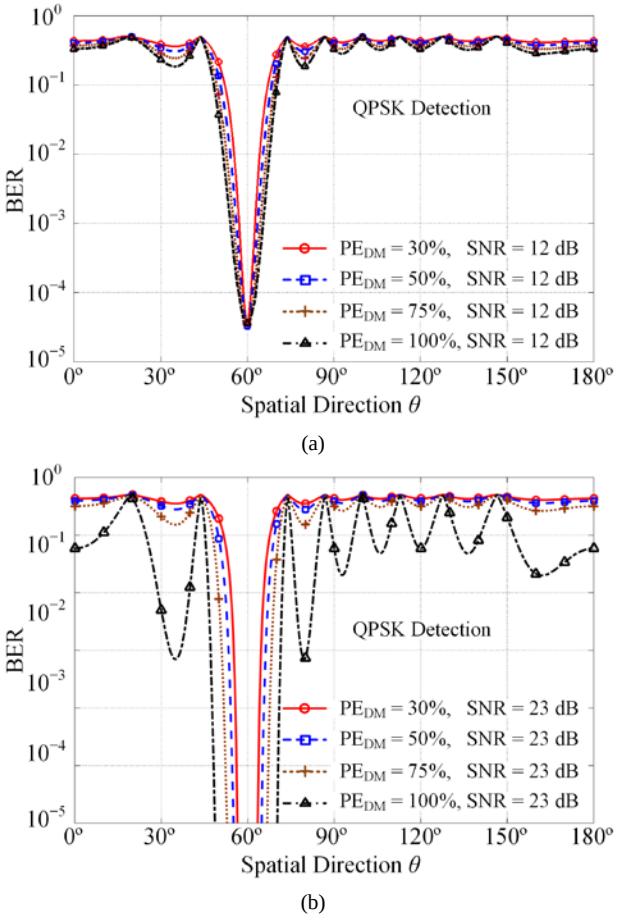

Fig. 4. Simulated BER spatial distributions for different PE_{DM}s in the example RDA DM system modulated for Gray-coded QPSK signal transmission. 10^{+7} random symbols are used in simulation. The PE_{DM} of 100% refers to the non-DM or classical RDA system. N = 9, α = 60°, and (a) SNR = 12 dB; (b) SNR = 23 dB.

For the two-legitimate-receiver case, the phase conjugated signal vector $\vec{U}_N$ can be written as

$$\vec{\boldsymbol{U}}_N = \begin{bmatrix} e^{-j\left[1-(N+1)/2\right]\pi\cos\alpha} + e^{-j\left\{\left[1-(N+1)/2\right]\pi\cos\beta+\varphi\right\}} \\ e^{-j\left[2-(N+1)/2\right]\pi\cos\alpha} + e^{-j\left\{\left[2-(N+1)/2\right]\pi\cos\beta+\varphi\right\}} \\ \vdots \\ e^{-j\left[N-(N+1)/2\right]\pi\cos\alpha} + e^{-j\left\{\left[N-(N+1)/2\right]\pi\cos\beta+\varphi\right\}} \end{bmatrix} \tag{9}$$

Here φ is the phase advance of the pilot signal from β than that of the pilot signal from α.

Using the same RDA DM transmitter structure shown in Fig. 1, and substituting (3) and (9) into (2), we get

$$\begin{aligned} \boldsymbol{P}(\theta) &= \underbrace{\vec{\boldsymbol{U}}_N \cdot \vec{\boldsymbol{F}}_N}_{\boldsymbol{P}_{info}} + \underbrace{\left(\vec{\boldsymbol{G}}_N \circ \vec{\boldsymbol{U}}_N\right)\cdot \vec{\boldsymbol{F}}_N}_{\boldsymbol{P}_{inter}} \\ &= \underbrace{\sum_{n=1}^{N}\left(e^{j\left[n-(N+1)/2\right]\pi(\cos\theta-\cos\alpha)} + e^{j\left\{\left[n-(N+1)/2\right]\pi(\cos\theta-\cos\beta)-\varphi\right\}}\right)}_{\boldsymbol{P}_{info}} \\ &\quad + \underbrace{\sum_{n=1}^{N}\left[\boldsymbol{G}_n\left(e^{j\left[n-(N+1)/2\right]\pi(\cos\theta-\cos\alpha)} + e^{j\left\{\left[n-(N+1)/2\right]\pi(\cos\theta-\cos\beta)-\varphi\right\}}\right)\right]}_{\boldsymbol{P}_{inter}} \end{aligned} \tag{10}$$

and

$$\begin{aligned} \boldsymbol{P}_{info}(\theta)\big|_{\theta=\alpha} &= N + e^{-j\varphi}\sum_{n=1}^{N} e^{j\left[n-(N+1)/2\right]\pi(\cos\alpha-\cos\beta)} \\ &= \begin{cases} N + e^{-j\varphi}\left[1+2\sum_{n=1}^{(N-1)/2}\cos(n\mu)\right] & \text{if } N \text{ is odd} \\ N + 2e^{-j\varphi}\left[\sum_{n=1}^{N-1}\cos(n\mu/2) - \sum_{n=1}^{N/2-1}\cos(n\mu)\right] & \text{if } N \text{ is even} \end{cases} \\ &= N + e^{-j\varphi}\cdot\frac{\sin(N\mu/2)}{\sin(\mu/2)} \end{aligned} \tag{11}$$

Here

$$\mu = \pi(\cos\alpha - \cos\beta), \qquad \mu \notin \{0, \pm 2\pi\} \tag{12}$$

If we design a network $\vec{\boldsymbol{G}}_N$ satisfying

$$\vec{\boldsymbol{G}}_N = \begin{cases} \boldsymbol{C}\cdot[\underbrace{-1\ \cdots\ -1}_{(N-1)/2\ items}\ 0\ \underbrace{1\ \cdots\ 1}_{(N-1)/2\ items}]^T & \text{if } N \text{ is odd} \\ \boldsymbol{C}\cdot[\underbrace{-1\ \cdots\ -1}_{N/2\ items}\ \underbrace{1\ \cdots\ 1}_{N/2\ items}]^T & \text{if } N \text{ is even} \end{cases} \tag{13}$$

where $\boldsymbol{C}$ can be any arbitrary complex number, the following can be derived;

$$\begin{aligned} \boldsymbol{P}_{inter}(\theta)\big|_{\theta=\alpha} &= \sum_{n=1}^{N}\left[\boldsymbol{G}_n\left(1+e^{j\left\{\left[n-(N+1)/2\right]\pi(\cos\alpha-\cos\beta)-\varphi\right\}}\right)\right] \\ &= \sum_{n=1}^{N}\boldsymbol{G}_n + e^{-j\varphi}\sum_{n=1}^{N}\left(\boldsymbol{G}_n e^{j\left[n-(N+1)/2\right]\mu}\right) \\ &= \begin{cases} 2je^{-j\varphi}\boldsymbol{C}\sum_{n=1}^{(N-1)/2}\sin(n\mu) & \text{if } N \text{ is odd} \\ 2je^{-j\varphi}\boldsymbol{C}\left[\sum_{n=1}^{N-1}\sin(n\mu/2) - \sum_{n=1}^{N/2-1}\sin(n\mu)\right] & \text{if } N \text{ is even} \end{cases} \\ &= \begin{cases} je^{-j\varphi}\boldsymbol{C}\dfrac{\cos(\mu/2)-\cos(N\mu/2)}{\sin(\mu/2)} & \text{if } N \text{ is odd} \\ je^{-j\varphi}\boldsymbol{C}\dfrac{1-\cos(N\mu/2)}{\sin(\mu/2)} & \text{if } N \text{ is even} \end{cases} \end{aligned} \tag{14}$$

In order to gain more insights into the relationship between $\boldsymbol{P}_{info}(\alpha)$ and $\boldsymbol{P}_{inter}(\alpha)$, the ratio $|\boldsymbol{P}_{info}(\alpha)/\boldsymbol{P}_{inter}(\alpha)|$ is plotted as a function of μ and φ in dB scale in Fig. 5. Both odd N and even N, 9 and 8 used as examples, are considered. Since parameter $\boldsymbol{C}$ only scales the $\boldsymbol{P}_{inter}(\alpha)$ in a linear fashion, see (14), it is held at unity in the examples shown in Fig. 5. When $\theta = \beta$, similar expressions to (11) and (14) can be obtained.

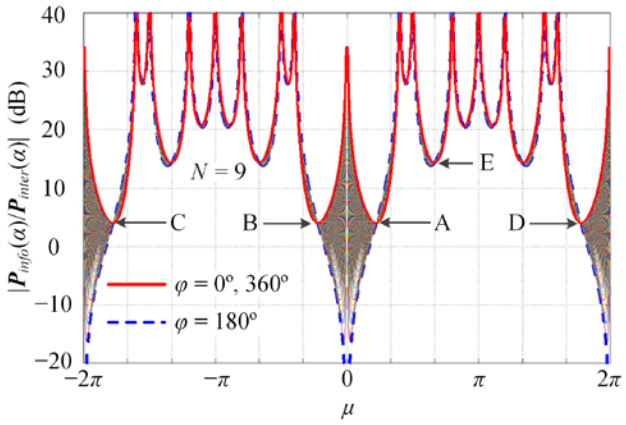

(a)

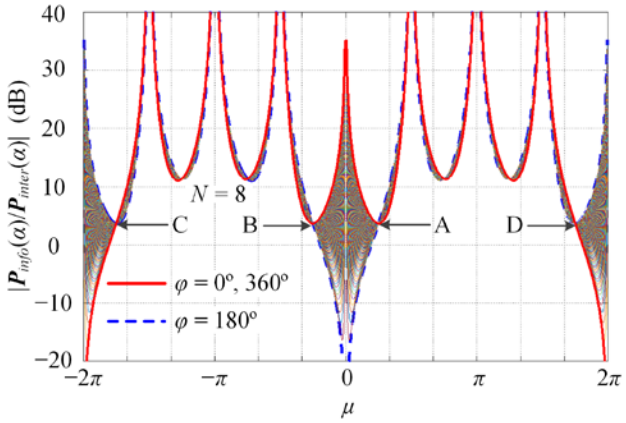

(b)

Fig. 5. Calculated example $|\boldsymbol{P}_{info}(\alpha)/\boldsymbol{P}_{inter}(\alpha)|$ as a function of μ and φ in dB scale. (a) $N = 9$; (b) $N = 8$.

In order to achieve DM functionality it is required that no, or at least very little, artificial interference energy is projected along selected communication direction(s). This then guarantees the preservation of the information signal waveform signatures detected by the legitimate receiver(s). Thus in Fig. 5 four critical points, A, B, C, and D, need to be identified, since when

$$\mu \in Q = (-2\pi, \mathrm{C}_x) \cup (\mathrm{B}_x, \mathrm{A}_x) \cup (\mathrm{D}_x, 2\pi) \tag{15}$$

the φ has great impact on the $|\boldsymbol{P}_{info}(\alpha)/\boldsymbol{P}_{inter}(\alpha)|$. Because the value of φ, i.e., the phase difference between two pilot tones, can be arbitrary in practice, region Q in (15) should be avoided in order to obtain large $|\boldsymbol{P}_{info}(\alpha)/\boldsymbol{P}_{inter}(\alpha)|$.

In order to facilitate discussion, letters, A, B, C, and D, with subscripts x and y refer to the abscissa and the ordinate values of their corresponding points in Fig. 5. It is interesting to note that when $\varphi = 0^{\circ}$ and $\mu \to 0$ the $|\boldsymbol{P}_{info}(\alpha)/\boldsymbol{P}_{inter}(\alpha)| \to +\infty$, indicating $|\boldsymbol{P}_{inter}(\alpha)| \to 0$. This scenario is actually the one interrogating device case presented in Section III.

The four critical points can be calculated from (16)

$$\frac{d\left[\left|\boldsymbol{P}_{info}(\alpha)/\boldsymbol{P}_{inter}(\alpha)\right|\right]}{d(\mu/2)} = 0 \tag{16}$$

Substituting (11) and (14) into (16), we get

$$\begin{cases} \sin(N\mu/2)\sin(\mu/2) = 0 & if\ \varphi = 0,\ N\ is\ odd \\ \tan(\mu/4)\tan(N\mu/4) = -N & if\ \varphi = 0,\ N\ is\ even \\ \cot(\mu/4)\tan(N\mu/4) = N & if\ \varphi = \pi,\ N\ is\ even \end{cases} \tag{17}$$

Upon considering $\mu \in (-2\pi, 0) \cup (0, 2\pi)$, the solutions of (17) are

$$\begin{cases} \mu = \pm\dfrac{2i\pi}{N} & (i = 1, 2, \cdots, N-1) & if\ \varphi = 0,\ N\ is\ odd \\ \mu \approx \pm\dfrac{2\pi + 4i\pi}{N} & \left(i = 0, 1, \cdots, \dfrac{N}{2} - 2\right) & if\ \varphi = 0,\ N\ is\ even \\ \mu \approx \pm\dfrac{2\pi + 4i\pi}{N} & \left(i = 1, 2, \cdots, \dfrac{N}{2} - 1\right) & if\ \varphi = \pi,\ N\ is\ even \end{cases} \tag{18}$$

By linking the solutions in (18) to the $|\boldsymbol{P}_{info}(\alpha)/\boldsymbol{P}_{inter}(\alpha)|$ curves in Fig. 5 four critical points can be identified,

$$\begin{cases} \mathrm{A}_x = \dfrac{2\pi}{N}, \mathrm{B}_x = -\dfrac{2\pi}{N}, \mathrm{C}_x = -\dfrac{2(N-1)\pi}{N}, \mathrm{D}_x = \dfrac{2(N-1)\pi}{N} \\ \qquad\qquad if\ N\ is\ odd \\ \mathrm{A}_x \approx \dfrac{2\pi}{N}, \mathrm{B}_x \approx -\dfrac{2\pi}{N}, \mathrm{C}_x \approx -\dfrac{2(N-1)\pi}{N}, \mathrm{D}_x \approx \dfrac{2(N-1)\pi}{N} \\ \qquad\qquad if\ N\ is\ even \end{cases} \tag{19}$$

It is worth noting that since $4\pi/N$ is the first null beamwidth (FNBW) in cosine domain in a classical beam steering array, solutions in (19) actually indicate that the two legitimate receivers need to be separated at least half FNBW in angle space.

Plotting (12) in Fig. 6, it can be seen that μ is a continuous and monotonic surface. Thus by setting μ of A_x, B_x, C_x, and D_x, the domain in which the (α, β) pairs satisfying $\mu \in \bar{Q}$ can be selected is shown as lying in the shaded areas in Fig. 7. When a $|\boldsymbol{P}_{info}(\alpha)/\boldsymbol{P}_{inter}(\alpha)|$ value of a DM system greater than A_y is required, the allowable μ region can be identified with the help of the $|\boldsymbol{P}_{info}(\alpha)/\boldsymbol{P}_{inter}(\alpha)|$ curves in Fig. 5. The projection of the allowable μ region in α-β plane set the area where (α, β) pairs could be chosen.

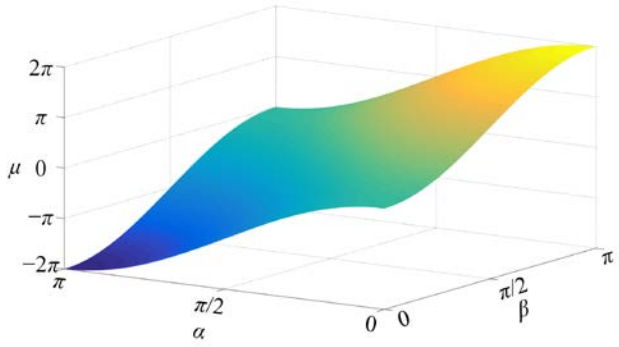

Fig. 6. μ as a function of α and β.

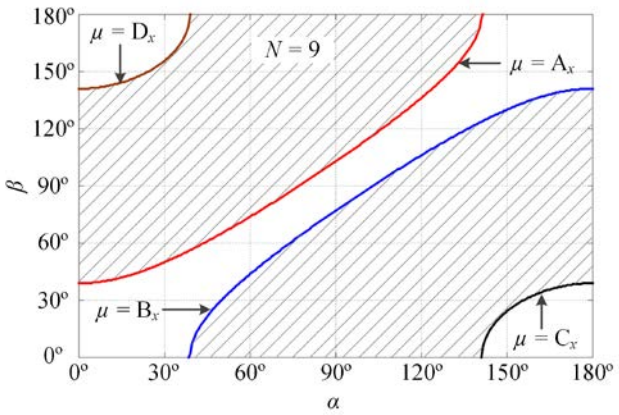

Fig. 7. Domain of acceptable (α, β) pairs for $|\boldsymbol{P}_{info}(\alpha)/\boldsymbol{P}_{inter}(\alpha)|$ greater than A_y (or B_y, C_y, D_y).

Revisiting (14), the perfect DM condition, i.e., $|\boldsymbol{P}_{inter}(\alpha)| = 0$, can be met when

$$\begin{cases}\cos(\mu/2)=\cos(N\mu/2) & \text{if } N \text{ is odd}\\ \cos(N\mu/2)=1 & \text{if } N \text{ is even}\end{cases}$$

$$\Rightarrow\begin{cases}\mu=\pm\dfrac{4i\pi}{N-1} & i=1,\cdots,\dfrac{N-3}{2} \quad \text{if } N \text{ is odd}\\ \mu=\pm\dfrac{4i\pi}{N+1} & i=1,\cdots,\dfrac{N-1}{2}\\ \mu=\pm\dfrac{4i\pi}{N} & i=1,\cdots,\dfrac{N}{2}-1 \quad \text{if } N \text{ is even}\end{cases} \tag{20}$$

Each value of μ represents a curve in (α-β) plane. Therefore there are infinite (α, β) pairs satisfying the perfect DM condition. For example, when N = 9, the perfect DM condition can be met by choosing (α, β) as (60º, 90º), (45º, 78º), or (60º, 84.2º), which correspond to μ of $\pi/2$, $\pi/2$, or $2\pi/5$, respectively. Fig. 8 depicts the calculated magnitude patterns of $\boldsymbol{P}_{info}(\theta)$ and $\boldsymbol{P}_{inter}(\theta)$ for different φ when N = 9 and (α, β) = (60º, 90º). As expected $|\boldsymbol{P}_{inter}|$ has two perfect power nulls along the selected α and β, irrespective of the values of φ. When φ = 90º there are no beam pointing errors of the two main beams in $|\boldsymbol{P}_{info}|$, as highlighted in Fig. 8. It has to be emphasized that even when φ is fixed the summed patterns $\boldsymbol{P}$ = $\boldsymbol{P}_{info}$ + $\boldsymbol{P}_{inter}$ along directions other than α and β can still be different since the phase of the complex number $\boldsymbol{C}$ in (13) can be arbitrarily selected. This is the key to scrambling signal waveforms along other directions. In Fig. 9 the calculated far-field patterns for 30 random QPSK symbols transmitted are shown. Here N = 9, (α, β) = (60º, 90º), and φ = 90º. For each symbol $|\boldsymbol{C}|$ is kept as unity and its phase is randomly chosen.

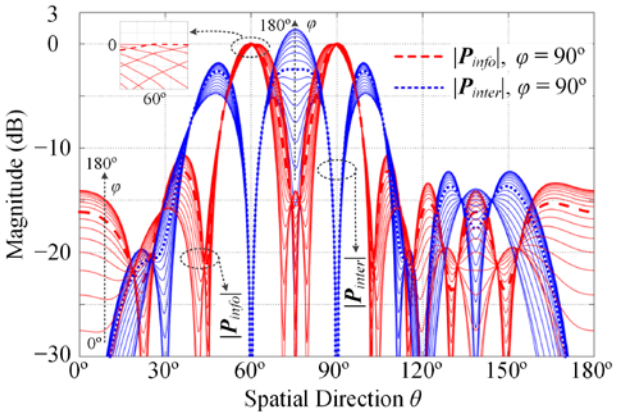

Fig. 8. Calculated magnitude patterns of $\boldsymbol{P}_{info}(\theta)$ and $\boldsymbol{P}_{inter}(\theta)$ for different φ when N = 9, (α, β) = (60º, 90º), and $|\boldsymbol{C}|$ = 1.

In Fig. 9 it can be observed that besides the required 60º and 90º directions, standard QPSK constellation patterns are also formed along 0º, 120º, and 180º, which is the consequence of additional perfect power nulls in $|\boldsymbol{P}_{inter}|$ along these three directions, see Fig. 8. However, as noticed in Fig. 9, the power along these directions is 16 dB less than that along the two legitimate receiver directions.

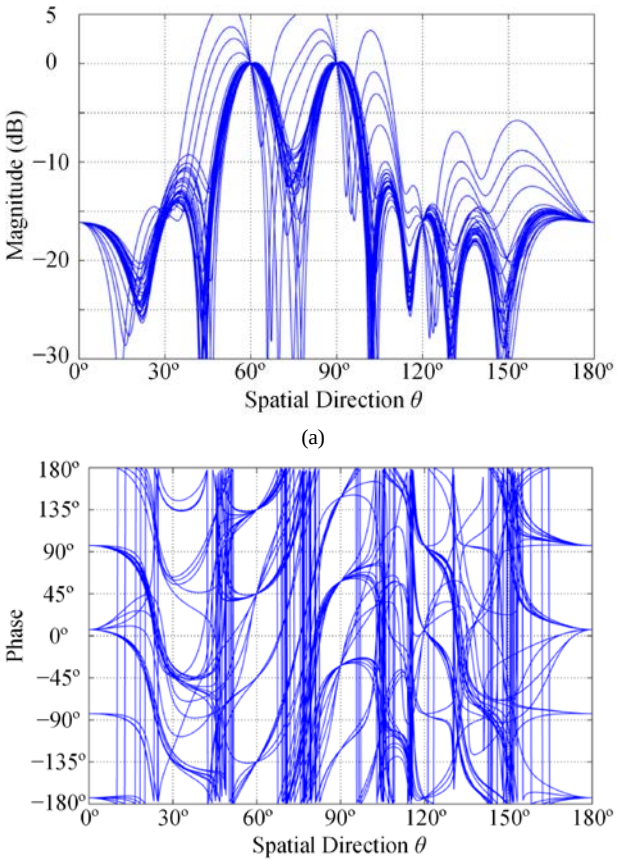

Fig. 9. Simulated far-field (a) magnitude and (b) phase patterns for 30 random QPSK symbols transmitted via the example RDA DM system. N = 9, (α, β) = (60º, 90º), φ = 90º, and $|\boldsymbol{C}|$ = 1.

BER simulation results of the example RDA DM system modulated for Gray-coded QPSK are obtained under different SNR scenarios, and are depicted in Fig. 10. Under the two-legitimate-receiver scenario, the system $\mathrm{PE}_{\mathrm{DM}}$ is a function of α, β, φ, and $\boldsymbol{C}$, see (21) to (25).

$$\mathrm{PE}_{\mathrm{DM}}=\frac{\int_{\theta=0}^{\theta=\pi}\left|\boldsymbol{P}_{info}\right|^2 d\theta}{\int_{\theta=0}^{\theta=\pi}\left|\boldsymbol{P}_{info}+\boldsymbol{P}_{inter}\right|^2 d\theta} \tag{21}$$

$$\boldsymbol{P}_{info}=\frac{\sin(N\xi_1/2)}{\sin(\xi_1/2)}+e^{-j\varphi}\frac{\sin(N\xi_2/2)}{\sin(\xi_2/2)} \tag{22}$$

$$\boldsymbol{P}_{inter}=\begin{cases}j\boldsymbol{C}\left[\dfrac{\cos(\xi_1/2)-\cos(N\xi_1/2)}{\sin(\xi_1/2)}+e^{-j\varphi}\dfrac{\cos(\xi_2/2)-\cos(N\xi_2/2)}{\sin(\xi_2/2)}\right] & \text{if } N \text{ is odd}\\ j\boldsymbol{C}\left[\dfrac{1-\cos(N\xi_1/2)}{\sin(\xi_1/2)}+e^{-j\varphi}\dfrac{1-\cos(N\xi_2/2)}{\sin(\xi_2/2)}\right] & \text{if } N \text{ is even}\end{cases} \tag{23}$$

$$\xi_1 = \pi\left(\cos\theta - \cos\alpha\right), \qquad \xi_1 \notin \{0, \pm 2\pi\} \tag{24}$$

$$\xi_2 = \pi\left(\cos\theta - \cos\beta\right), \qquad \xi_2 \notin \{0, \pm 2\pi\} \tag{25}$$

When α, β, and φ are fixed, the choice of $|\boldsymbol{C}|$ determines the system PE_{DM}. Again as predicted, seen in Fig. 10, the greater the value of $|\boldsymbol{C}|$, i.e., the lower the PE_{DM}, the narrower the two BER main beams become and the higher the BER sidelobes are, except along the three directions, i.e., 0º, 120º, and 180º, as discussed in the last paragraph. The '$|\boldsymbol{C}| = 0$' case refers to the classical RDA operation, i.e., $PE_{DM} = 100\%$.

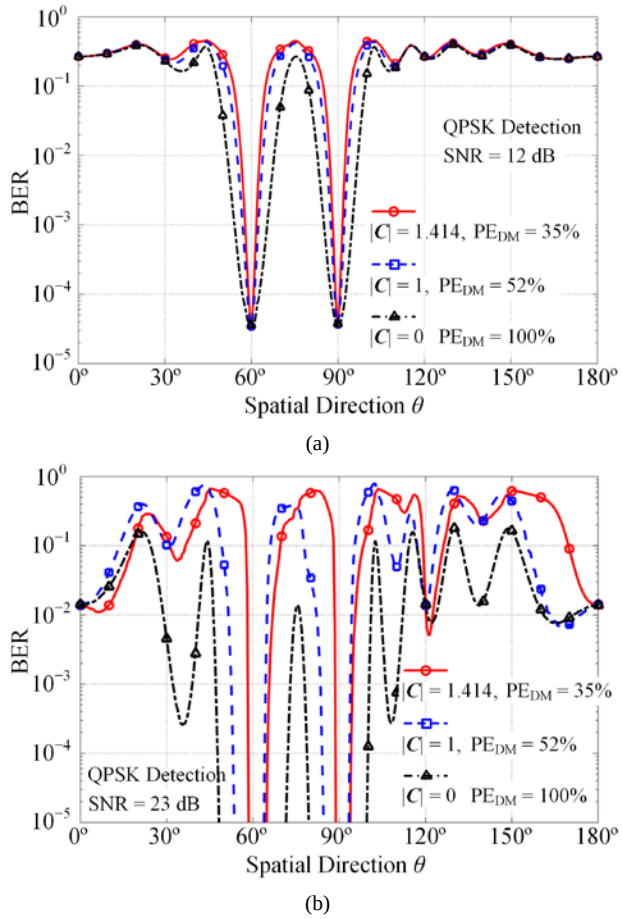

Fig. 10. Simulated BER spatial distributions for different $|\boldsymbol{C}|$ in the example RDA DM system modulated for Gray-coded QPSK signal transmission. 10^{+7} random symbols are used in simulation. The $|\boldsymbol{C}|$ of 0 refers to the non-DM or classical RDA system. $N = 9$, $(\alpha, \beta) = (60º, 90º)$, $\varphi = 90º$, and (a) SNR = 12 dB; (b) SNR = 23 dB.

Another example of $|\boldsymbol{P}_{info}(\theta)|$ and $|\boldsymbol{P}_{inter}(\theta)|$ for the RDA DM system with $N = 9$ and $(\alpha, \beta) = (60º, 99.6º)$ is shown in Fig. 11. Here $\mu = \pi(\cos\alpha - \cos\beta) = 2\pi/3$, corresponding to one of the lowest $|\boldsymbol{P}_{info}(\alpha)/\boldsymbol{P}_{inter}(\alpha)|$ sidelobes, i.e., point E in Fig. 5(a). Unlike the characteristic of perfect orthogonality between $|\boldsymbol{P}_{info}|$ and $|\boldsymbol{P}_{inter}|$ along α and β shown in Fig. 8, $|\boldsymbol{P}_{inter}(\alpha)|$ and $|\boldsymbol{P}_{inter}(\beta)|$ are no longer zero in Fig. 11. In this example they are 14.3 dB lower than $|\boldsymbol{P}_{info}(\alpha)|$ and $|\boldsymbol{P}_{info}(\beta)|$, see both Fig. 5(a) and Fig. 11. This non-perfect orthogonality property, on the other hand, eliminates the power nulls in $|\boldsymbol{P}_{inter}(\theta)|$ for most φ values along other directions, which always exist for perfect orthogonality DM systems such as the one in Fig. 8. Therefore there is a trade-off between the signal quality along the selected communication directions and the amount of information leakage along other directions. Fig. 12 illustrates simulated far-field patterns when 30 random QPSK symbols are transmitted via the example RDA DM array. Again φ is set to 90º and $|\boldsymbol{C}|$ as unity. It can be seen in Fig. 12 that the detected QPSK signal formats are slightly distorted along the desired communication directions α and β. This minute disturbance acts as interference, as a consequence, requiring a small amount of extra information signal power for the detection of the same levels of BER in the corresponding non-DM systems, i.e., $|\boldsymbol{C}| = 0$. For example, when $|\boldsymbol{C}| = 1.414$, an extra 0.8 dB signal power is needed to compensate the introduced interference along α and β, resulting in an equivalent signal to interference plus noise ratio (SINR) of 12 dB. See the example in Fig. 13(a). This, however, provides an opportunity of suppressing BER sidelobes along all other directions, which can be observed under the higher SNR scenario shown in Fig. 13(b). These observations provide a guideline on the choice of $|\boldsymbol{C}|$ when a practical system design is considered. For the example in Fig. 13, if the system requires at least 3.4×10^{-5} BER at legitimate receiver sides (corresponding to SNR of 12 dB in the non-DM system) and an allowable maximum 0.8 dB increase in information signal power compared with that in the non-DM system, then the upper limit of the choice of $|\boldsymbol{C}|$ is 1.414.

It is worth noting that the same value of $|\boldsymbol{C}|$ for different receivers' settings normally results in different system PE_{DM}s, see Fig. 10, Fig. 13, and Fig. 17.

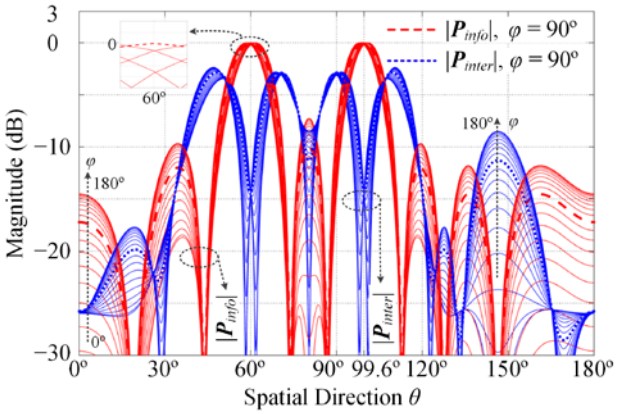

Fig. 11. Calculated magnitude patterns of $\boldsymbol{P}_{info}(\theta)$ and $\boldsymbol{P}_{inter}(\theta)$ for different φ when $N = 9$, $(\alpha, \beta) = (60º, 99.6º)$, and $|\boldsymbol{C}| = 1$.

The above analysis in this section can be extended for the scenarios where more than two, but less than N–1, legitimate receivers interrogating the proposed RDA DM transmitters. The limit of N–1 comes from the fact that an N-element linear array can form a maximum number of N–1 radiation main beams in half space.

Assume that there are M legitimate receivers located along different spatial directions, $2 \le M \le N$–1, and the network $\bar{\boldsymbol{G}}_N$ in the synthesis-free RDA DM transmitter is still designed as in

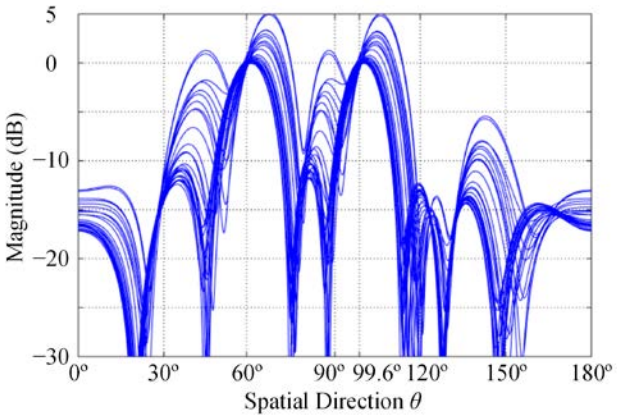

(a)

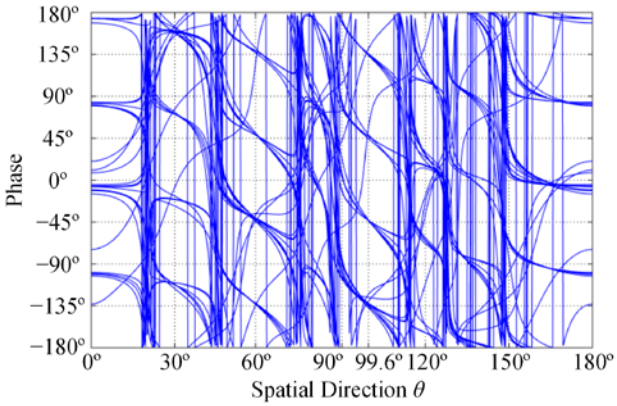

(b)

Fig. 12. Simulated far-field (a) magnitude and (b) phase patterns for 30 random QPSK symbols transmitted via the example RDA DM system. N = 9, (α, β) = (60º, 99.6º), φ = 90º, and $|\boldsymbol{C}|$ = 1.

(13). Following the similar derivation procedures as for the two-receiver case, the generalized $\boldsymbol{P}(\theta)$, as well as separated $\boldsymbol{P}_{info}(\theta)\big|_{\theta=\theta_i}$ and $\boldsymbol{P}_{inter}(\theta)\big|_{\theta=\theta_i}$, can be obtained as in (26) to (28). Here θ_i or θ_m denotes the incident angle of the pilot tone from the i^{th} or m^{th} legitimate receiver, (i, $m \in (1, \ldots, M)$).

$$\begin{aligned}\boldsymbol{P}(\theta) &= \underbrace{\vec{\boldsymbol{U}}_N \cdot \vec{\boldsymbol{F}}_N}_{\boldsymbol{P}_{info}} + \underbrace{\left(\vec{\boldsymbol{G}}_N \circ \vec{\boldsymbol{U}}_N\right)\cdot \vec{\boldsymbol{F}}_N}_{\boldsymbol{P}_{inter}} \\ &= \underbrace{\sum_{n=1}^{N}\sum_{m=1}^{M} e^{j\left\{\left\lceil n-(N+1)/2\right\rceil \pi(\cos\theta-\cos\theta_m)-\varphi_m\right\}}}_{\boldsymbol{P}_{info}} \\ &\quad + \underbrace{\sum_{n=1}^{N}\left(\boldsymbol{G}_n \sum_{m=1}^{M} e^{j\left\{\left\lceil n-(N+1)/2\right\rceil \pi(\cos\theta-\cos\theta_m)-\varphi_m\right\}}\right)}_{\boldsymbol{P}_{inter}}\end{aligned} \tag{26}$$

$$\begin{aligned}\boldsymbol{P}_{info}(\theta)\big|_{\theta=\theta_i} &= Ne^{-j\varphi_i} + \sum_{n=1}^{N}\sum_{\substack{m=1\\ m\neq i}}^{M} e^{j\left\{\left\lceil n-(N+1)/2\right\rceil \pi(\cos\theta_i-\cos\theta_m)-\varphi_m\right\}} \\ &= Ne^{-j\varphi_i} + \sum_{\substack{m=1\\ m\neq i}}^{M} e^{-j\varphi_m}\cdot\frac{\sin\left(N\mu_{im}/2\right)}{\sin\left(\mu_{im}/2\right)}\end{aligned} \tag{27}$$

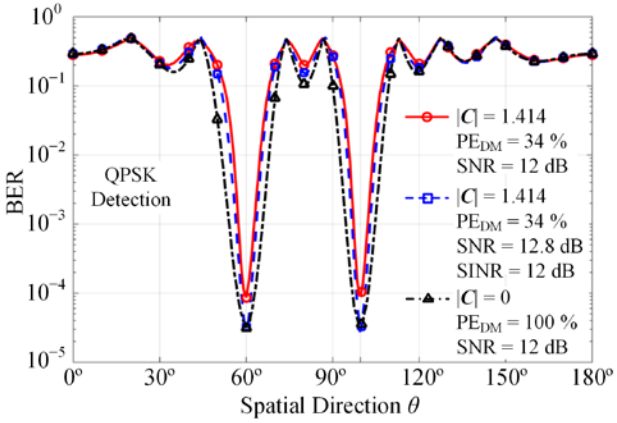

(a)

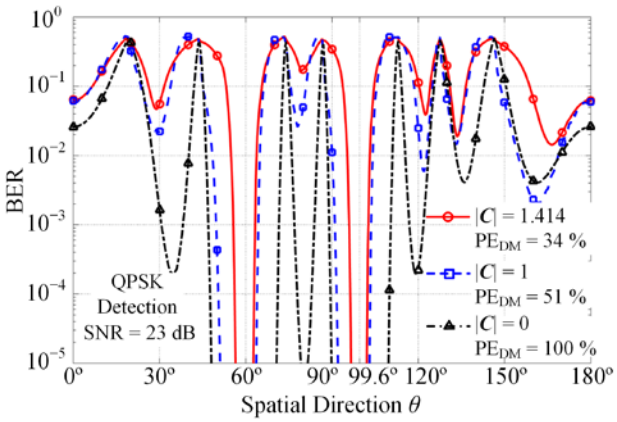

(b)

Fig. 13. Simulated BER spatial distributions for different $|\boldsymbol{C}|$ in the example RDA DM system modulated for Gray-coded QPSK signal transmission. 10^{+7} random symbols are used in simulation. The $|\boldsymbol{C}|$ of 0 refers to the non-DM or classical RDA system. N = 9, (α, β) = (60º, 99.6º), φ = 90º, and (a) SNR = 12 dB and 12.8 dB; (b) SNR = 23 dB.

$$\boldsymbol{P}_{inter}(\theta)\big|_{\theta=\theta_i} = \begin{cases} j\boldsymbol{C}\sum_{\substack{m=1\\ m\neq i}}^{M}\left(e^{-j\varphi_m}\dfrac{\cos\left(\mu_{im}/2\right)-\cos\left(N\mu_{im}/2\right)}{\sin\left(\mu_{im}/2\right)}\right) & \text{if } N \text{ is odd} \\ j\boldsymbol{C}\sum_{\substack{m=1\\ m\neq i}}^{M}\left(e^{-j\varphi_m}\dfrac{1-\cos\left(N\mu_{im}/2\right)}{\sin\left(\mu_{im}/2\right)}\right) & \text{if } N \text{ is even}\end{cases} \tag{28}$$

$$\mu_{im} = \pi\left(\cos\theta_i - \cos\theta_m\right), \qquad \mu_{im} \notin \{0, \pm 2\pi\} \tag{29}$$

The φ_i or φ_m are the phase differences of the i^{th} or m^{th} pilot tone signals relative to the phase of the first one, thus φ_1 = 0.

Similarly the $|\boldsymbol{P}_{info}(\theta_i)/\boldsymbol{P}_{inter}(\theta_i)|$ can be calculated, which is a function of μ_{im} and φ_m. By setting a minimum threshold of the $|\boldsymbol{P}_{info}(\theta_i)/\boldsymbol{P}_{inter}(\theta_i)|$, the acceptable μ_{im}, and hence the selectable (θ_1, θ_2, …, θ_M), with the help of the functions or surfaces described in (29), can then be identified. Since these procedures have recourse to multi-dimensional graphs which are difficult to be presented in the paper, the associated contents are omitted here. In Fig. 14 two typical results of the calculated far-field magnitude patterns, both information patterns $|\boldsymbol{P}_{info}|$ and

interference patterns $|\boldsymbol{P}_{inter}|$, generated by the proposed 9-element RDA DM transmitters for three-legitimate-receiver case are presented. When $(\theta_1, \theta_2, \theta_3) = (60^o, 90^o, 120^o)$, corresponding to $(\mu_{12}, \mu_{13}, \mu_{23}) = (\pi/2, \pi, -\pi/2)$, the $|\boldsymbol{P}_{info}|$ and $|\boldsymbol{P}_{inter}|$ are perfectly orthogonal along the three selected directions, see Fig. 14(a), which can be further validated by substituting the values of $(\mu_{12}, \mu_{13}, \mu_{23})$ into (23) that returns 0. While in Fig. 14(b) the choice of $(\theta_1, \theta_2, \theta_3) = (60^o, 90^o, 150^o)$ results in non-perfectly orthogonal $|\boldsymbol{P}_{info}|$ and $|\boldsymbol{P}_{inter}|$. BER simulation results for multi-receiver RDA DM systems, under various choices of $|\boldsymbol{C}|$ that links to PE_{DM}s, exhibit the same characteristics as those for the two-receiver case, thus they are omitted here.

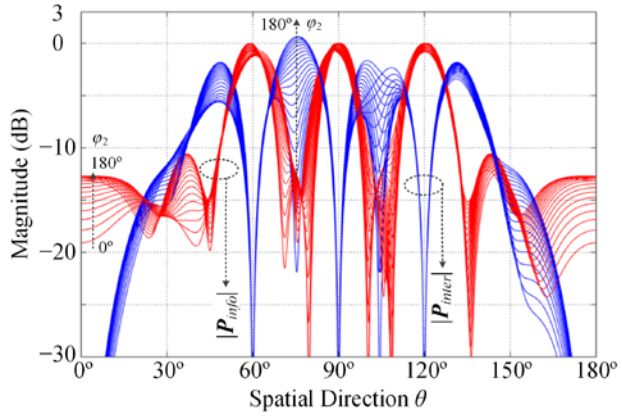

(a)

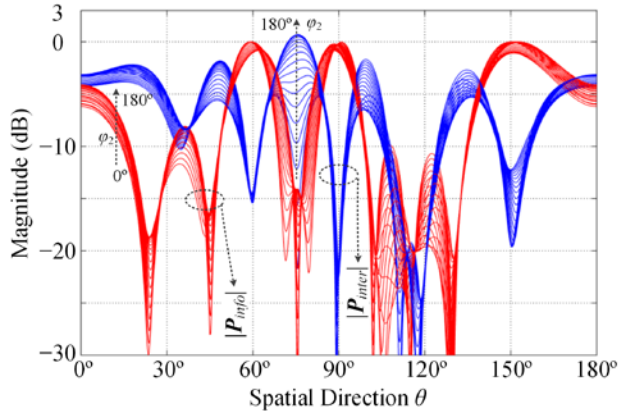

(b)

Fig. 14. Calculated magnitude patterns of $\boldsymbol{P}_{info}(\theta)$ and $\boldsymbol{P}_{inter}(\theta)$ for different φ_2 when $N = 9$, $\varphi_3 = 90^o$, $|\boldsymbol{C}| = 1$, and (a) $(\theta_1, \theta_2, \theta_3) = (60^o, 90^o, 120^o)$; (b) $(\theta_1, \theta_2, \theta_3) = (60^o, 90^o, 150^o)$.

V. Validation in Multipath Environment

The applicability of the proposed RDA DM architecture in the free space multiple-legitimate-receiver scenarios gives us a hint that it should operate in a multipath environment. The only difference for the multipath case is that the re-transmitted signals along different propagation paths are required to be constructively combined at legitimate receiver location(s). Fortunately, this is automatically guaranteed because it is the inherent property that an RDA possesses [43].

Firstly in this section a simplified two-ray multipath model, used previously in [24], is adopted to demonstrate the multipath compatibility of the proposed synthesis-free RDA DM transmitter. The DM enabling network $\vec{\boldsymbol{G}}_N$ is designed as in (13). The two-ray model is illustrated in Fig. 15. In this example an intended receiver is located along boresight of a 9-element half wavelength ($\lambda/2$) spaced linear RDA DM transmitter array at a line-of-sight distance of 100λ. By placing an infinite-sized perfect reflector perpendicular to the array, each point in the two-dimensional (2-D) ring-like simulation area, from a radius of 90λ to 200λ, can receive two rays. One is received directly from line-of-sight, and the other is routed through reflection. The path loss differences of each ray are considered.

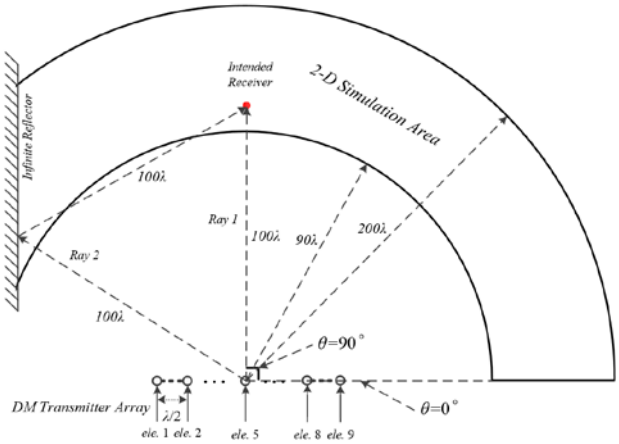

Fig. 15. Simplified two-ray multipath model.

When a pilot tone signal is isotropically emitted by the intended receiver, two rays from the paths *Ray1* and *Ray2* , seen in Fig. 15, in reverse directions impinge upon the RDA DM transmitter array, exciting re-transmitted information and interference patterns, $\boldsymbol{P}_{info}$ and $\boldsymbol{P}_{inter}$. Their magnitudes for $|\boldsymbol{C}| = 1$ are depicted in Fig. 16. From the $|\boldsymbol{P}_{info}|$ curve it can be observed that the reflection beam around 150^o is 6 dB lower than the boresight beam. This is because *Ray2* path length is twice as long as *Ray1*. The two pilot rays detected at the transmitter side are in-phase, which results in beam pointing errors of the re-transmitted two beams, see discussions on φ for two-receiver case in Section IV.

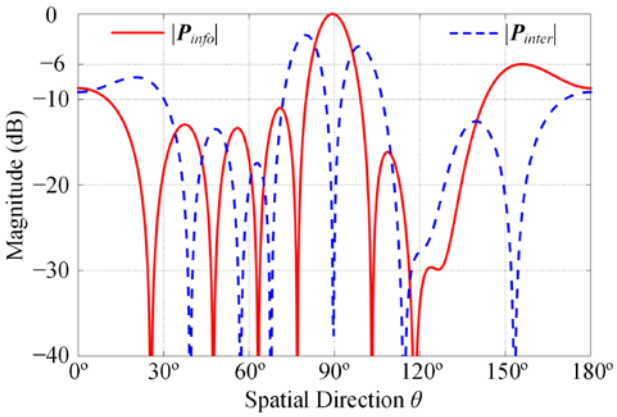

Fig. 16. Calculated magnitudes of re-transmitted information and interference patterns, $|\boldsymbol{P}_{info}|$ and $|\boldsymbol{P}_{inter}|$, by the RDA DM transmitter in Fig. 15. $N = 9$ and $|\boldsymbol{C}| = 1$.

BER simulations for Gray-coded QPSK transmission were conducted under the SNR of 23 dB for different values of $|\boldsymbol{C}|$, from which the system PE_{DM}s can be calculated using (21) to (23) with a coefficient 0.5 being added before $e^{-j\varphi}$, accounting for the path loss difference between two rays in this example system. The results are shown in Fig. 17. The 23 dB SNR at intended receiver location was chosen to facilitate clear illustrations of 2-D BER distributions in grey-scale. The AWGN contribution is assumed to be identical over the entire simulation area.

From the obtained BER results in Fig. 17, it can be seen that the proposed RDA DM transmitter is able to securely convey information signals to the intended receiver, with signals detected at most other locations being seriously distorted, resulting in high BERs. The greater the selected $|\boldsymbol{C}|$, i.e., the smaller the system PE_{DM}, the smaller the error-free zone becomes. It is interesting to point out that the error-free zone around 150º cannot be eliminated by increasing the value of $|\boldsymbol{C}|$, since no interference can be projected into this area, see the power null around 150º in $|\boldsymbol{P}_{inter}|$ in Fig. 16.

This is different to the DM systems synthesized by the orthogonal vector approach in [21], wherein useful signals are chopped into pieces and each piece is transmitted along different propagation paths with constructive combination occurring only at the legitimate receiver location. While in the synthesis-free RDA DM systems proposed in this paper, instead of information signal pieces, the weighted copies of useful information signals are projected along different propagation paths with in-phase combination enabled only at the legitimate receiver location. As a consequence, when no interference energy can be delivered into the routes through which the copies of information signals travel between the transmitter and the intended receiver from other propagation paths, the unscrambled information signal waveforms can be detected within these areas, e.g., the area around 150º in Fig. 17.

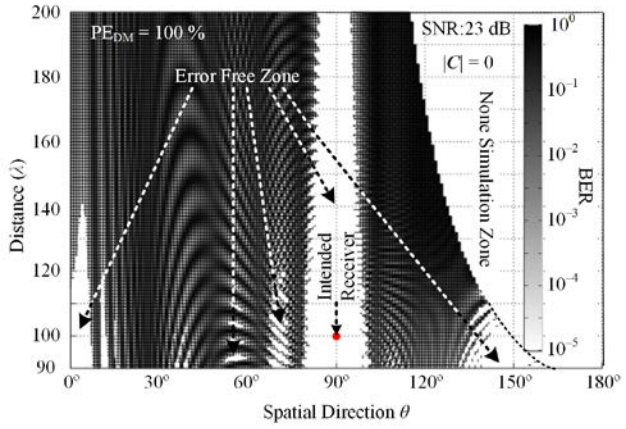

(a)

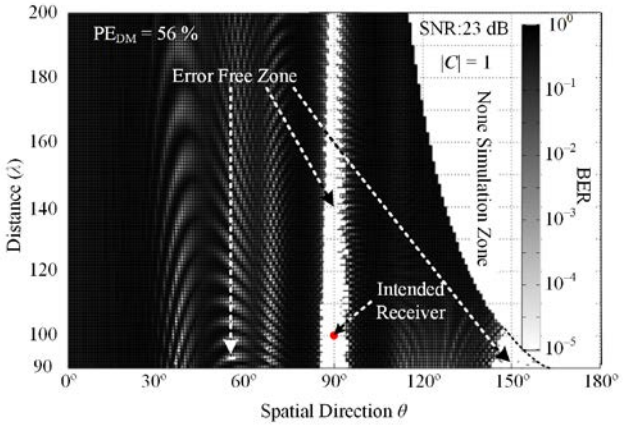

(b)

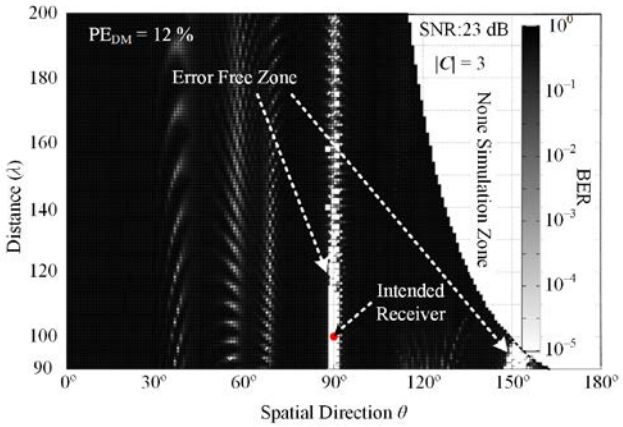

(c)

Fig. 17. Simulated 2-D BER distributions for different $|\boldsymbol{C}|$ in the example RDA DM system in the two-ray multipath environment. The array is modulated for Gray-coded QPSK signal transmission. 10^{+7} random symbols are used in simulation. None simulation zone is the area blocked by the infinite perfect reflector. The $|\boldsymbol{C}|$ of 0 refers to the non-DM or classical RDA system. N = 9, SNR = 23 dB, and (a) $|\boldsymbol{C}|$ = 0, PE_{DM} = 100%; (b) $|\boldsymbol{C}|$ = 1, PE_{DM} = 56%; (c) $|\boldsymbol{C}|$ = 3, PE_{DM} = 12%.

In order to further investigate the performance of the proposed RDA DM system in multipath-rich environment, a metal shielded cube of 2.5×2.5×2.5 m^3, in which a 7-element RDA DM array with $\lambda/2$ spacing, operating at f = 2.4 GHz, is placed, is considered. A square metal sheet with a size of 1.5×1.5 m^2 is inserted between the transmitter and the interested 2-D simulation area to block line-of-sight rays. The detailed model parameters are labelled in Fig. 18. The wave propagation software WinProp version 11.06 [44] was used to generate the transmission coefficients between each transmit antenna element and each point in the 2-D 1×2.5 m^2 simulation area. All of the metallic plates have their reflection loss set to be 0.05 dB and the diffraction loss is constrained to lie between 8 and 15 dB. In the simulation up to 100 rays with largest energy between each transmit antenna and each point in the simulation area are obtained, and then summed to get the transmission coefficients.

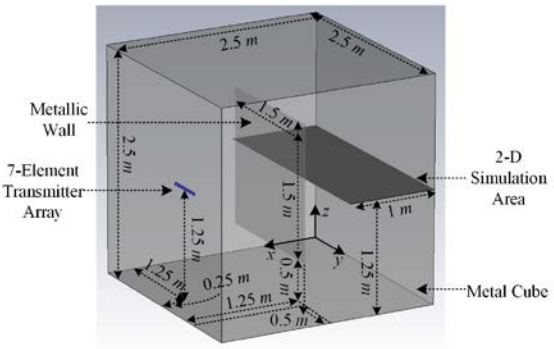

Fig. 18. Metal shielded cube model for multipath-rich wireless transmission.

With the computed transmission coefficients between each of the seven antenna elements and each point on the 2-D simulation area, BER simulations can be performed under various transmitter, i.e., different $|\boldsymbol{C}|$ values, and receiver settings. Again it is assumed that the network $\vec{\boldsymbol{G}}_N$ in the RDA DM transmitter takes the form in (13) and the re-transmitted signals are modulated for Gray-coded QPSK. Three different scenarios, with regard to the number of intended receivers and its or their location(s), are investigated. Under the first scenario only one intended receiver located at the geometric center of the 2-D simulation area is considered, i.e., the point of $(x, y, z) = (0.5m, 1.25m, 1.25m)$. In the second and the third scenarios two intended receivers, being placed, respectively, in a symmetrical and an asymmetrical fashion, are considered. The pilot signals radiated by the two legitimate receivers are assumed to be isotropic and have identical power. The phase difference between them can be arbitrarily selected, and is set to 0 for the examples illustrated below.

Simulated BER distributions under the single receiver scenario are shown in Fig. 19 for various choices of $|\boldsymbol{C}|$. Since a large number of rays exist in this example system, the calculation of system PE_{DM}s is complicated, thus they are not presented. However, when the choice of receivers is made, then larger values of $|\boldsymbol{C}|$ always result in lower PE_{DM}s. The SNRs detected by the desired receiver are set to be 20 dB. It can be seen that the proposed synthesis-free RDA DM array has considerable ability to distort the leaked information signals at other locations, resulting in high BER values. While at the position where the intended receiver locates, the artificial interference generated by the synthesis-free network $\vec{\boldsymbol{G}}_N$ stays largely orthogonal to the information signal, since only when $|\boldsymbol{C}|$ is as large as 13 the impact of the interference on BER can be visible.

The same conclusion can be drawn for the second scenario, i.e., two legitimate receivers locate at $(0.5m, 0.625m, 1.25m)$ and $(0.5m, 1.875m, 1.25m)$, see BER simulation results in Fig. 20. The involvement of more number of desired receivers, as expected, degrades the orthogonality between information and artificial interference. In this example, when $|\boldsymbol{C}|$ increases to 8, bit errors can be detected by the two intended receivers under SNR of 20 dB.

The third scenario is slightly different since the two desired receivers are asymmetrically placed at $(0.25m, 1.25m, 1.25m)$ and $(0.5m, 0.469m, 1.25m)$. They are labelled as R1 and R2, respectively. It is noted here that the value of 0.469 corresponds to the 30^{th} pixel out of total 160 pixels, into which the simulation area is divided along y axis, i.e., $0.469 = 2.5/160\times30$. Since R1 and R2 are asymmetrically placed, the power of information signals delivered to them is different. In this example the detected information power, hence the SNR, by R1 is 3.7 dB higher than that detected by R2. Thus bit errors appear first at R2 along with the increase of the parameter $|\boldsymbol{C}|$, see Fig. 21 for SNR of 20 dB at R1.

VI. Discussion on Hardware Implementation

As we presented from Section II to V, it is the network $\vec{\boldsymbol{G}}_N$ augmented onto a classical RDA that enables the synthesis-free DM functionality in a number of application scenarios. Its mathematical form in (13) for multi-receiver applications satisfies the one in (5) for single receiver case, thus (13) is the preferred choice in terms for realization. From a hardware implementation perspective, (13) can be realized using an $N-1$ or N-channel fixed phase delay network, corresponding to the vector $[-1 \quad \cdots \quad 1]^T$, and one gain- and phase-reconfigurable component, corresponding to the variable $\boldsymbol{C}$. It is worth noting that the variable component can have very poor precision since it does not affect the orthogonality between the information and the generated artificial interference. The practical realization and operating characteristics of the RDA DM architecture will be reported separately.

VII. Conclusion

A practical DM transmitter architecture was proposed in this paper. Built upon classical RDA technology, it requires only a few low-complex hardware augments. The proposed RDA DM transmitter has the unique capability that it can operate without any prior knowledge of how many and where the desired receivers lie even in heavily multipath-rich environments. The effectiveness of the proposed RDA DM system was validated through simulation under various application scenarios, among which the multi-receiver multipath operation paves a way for future field use of DM technology in areas where physical-layer wireless security offers additional, or security augmentation, benefits over conventionally secured systems.

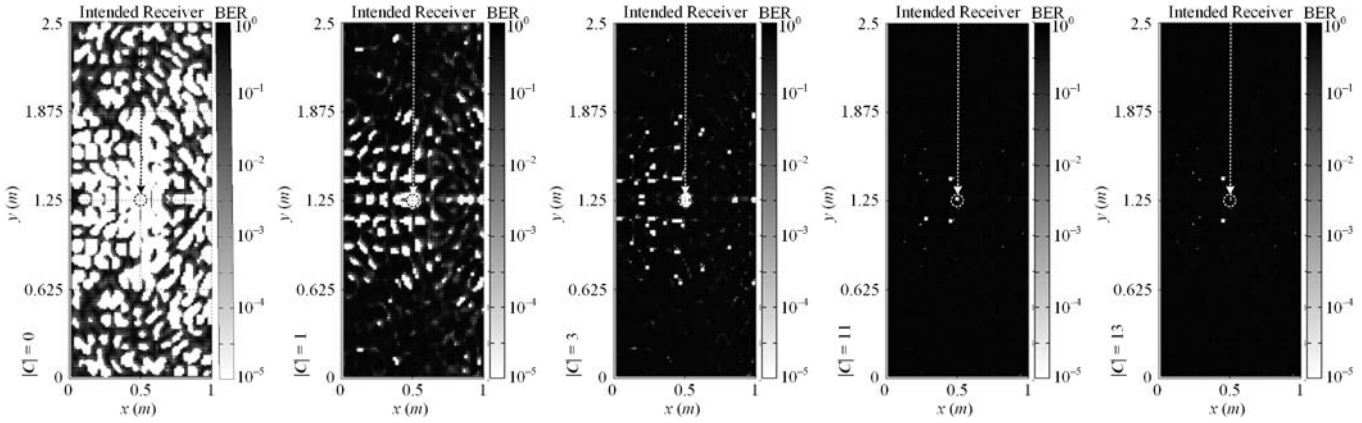

(a) (b) (c) (d) (e)

Fig. 19. Simulated 2-D BER distributions for different $|\boldsymbol{C}|$ in the example RDA DM system in the multipath-rich cube environment. The array is modulated for Gray-coded QPSK signal transmission. 10^{+7} random symbols are used in simulation. Only one intended receiver locates at (0.5m, 1.25m, 1.25m). The $|\boldsymbol{C}|$ of 0 refers to the non-DM or classical RDA system. N = 7, f = 2.4 GHz, SNR = 20 dB, and (a) $|\boldsymbol{C}|$ = 0; (b) $|\boldsymbol{C}|$ = 1; (c) $|\boldsymbol{C}|$ = 3; (d) $|\boldsymbol{C}|$ = 11; (e) $|\boldsymbol{C}|$ = 13.

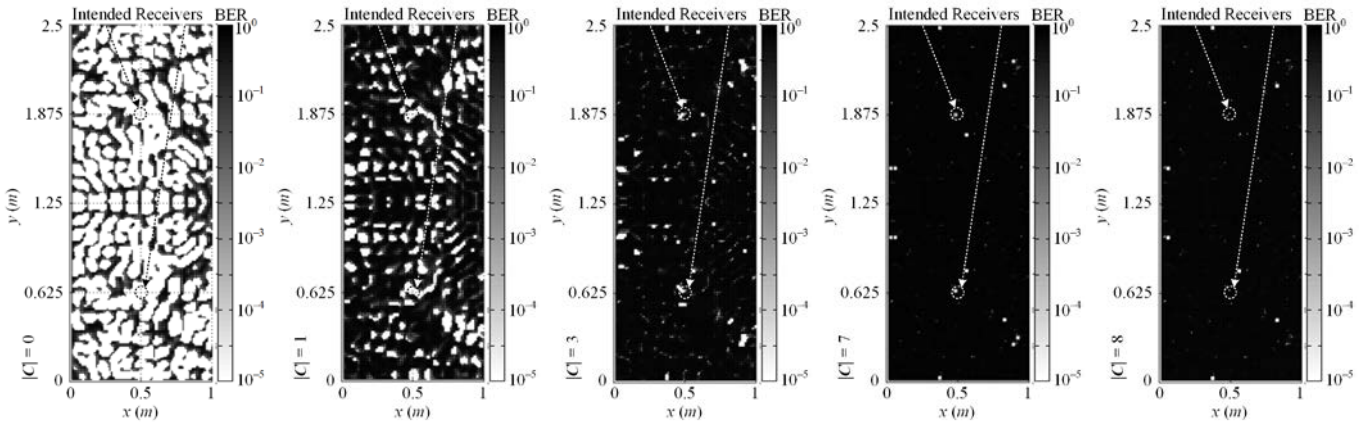

(a) (b) (c) (d) (e)

Fig. 20. Simulated 2-D BER distributions for different $|\boldsymbol{C}|$ in the example RDA DM system in the multipath-rich cube environment. The array is modulated for Gray-coded QPSK signal transmission. 10^{+7} random symbols are used in simulation. Two intended receivers locate at (0.5m, 0.625m, 1.25m) and (0.5m, 1.875m, 1.25m). The $|\boldsymbol{C}|$ of 0 refers to the non-DM or classical RDA system. N = 7, f = 2.4 GHz, φ = 0, SNR = 20 dB, and (a) $|\boldsymbol{C}|$ = 0; (b) $|\boldsymbol{C}|$ = 1; (c) $|\boldsymbol{C}|$ = 3; (d) $|\boldsymbol{C}|$ = 7; (e) $|\boldsymbol{C}|$ = 8.

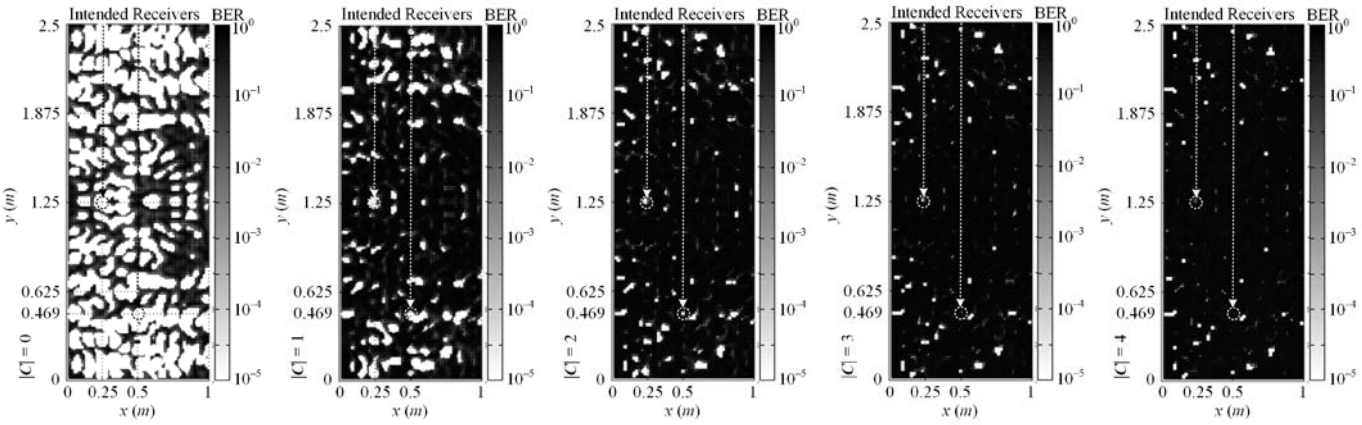

(a) (b) (c) (d) (e)

Fig. 21. Simulated 2-D BER distributions for different $|\boldsymbol{C}|$ in the example RDA DM system in the multipath-rich cube environment. The array is modulated for Gray-coded QPSK signal transmission. 10^{+7} random symbols are used in simulation. Two intended receivers R1 and R2 locate at (0.25m, 1.25m, 1.25m) and (0.5m, 0.469m, 1.25m). The $|\boldsymbol{C}|$ of 0 refers to the non-DM or classical RDA system. N = 7, f = 2.4 GHz, φ = 0, SNR = 20 dB at R1, and (a) $|\boldsymbol{C}|$ = 0; (b) $|\boldsymbol{C}|$ = 1; (c) $|\boldsymbol{C}|$ = 2; (d) $|\boldsymbol{C}|$ = 3; (e) $|\boldsymbol{C}|$ = 4.

REFERENCES

[1] Y. Ding and V. Fusco, "A vector approach for the analysis and synthesis of directional modulation transmitters," *IEEE Trans. Antennas Propag.* vol. 62, no. 1, pp. 361–370, Jan. 2014.

[2] A. Babakhani, D. B. Rutledge, and A. Hajimiri, "Transmitter architectures based on near-field direct antenna modulation," *IEEE J. Solid-State Circuits*, vol. 43, no. 12, pp. 2674–2692, Dec. 2008.

[3] A. Babakhani, D. Rutledge, and A. Hajimiri, "Near-field direct antenna modulation," *IEEE Microw. Mag.*, vol. 10, no. 1, pp. 36–46, Feb. 2009.

[4] M. P. Daly and J. T. Bernhard, "Beamsteering in pattern reconfigurable arrays using directional modulation," *IEEE Trans. Antennas Propag.*, vol. 58, no. 7, pp. 2259–2265, Jul. 2010.

[5] M. P. Daly and J. T. Bernhard, "Directional modulation technique for phased arrays," *IEEE Trans. Antennas Propag.*, vol. 57, no. 9, pp. 2633–2640, Sept. 2009.

[6] M. P. Daly, E. L. Daly, and J. T. Bernhard, "Demonstration of directional modulation using a phased array," *IEEE Trans. Antennas Propag.*, vol. 58, no. 5, pp. 1545–1550, May 2010.

[7] H. Shi and A. Tennant, "Direction dependent antenna modulation using a two element array," in *Proc. 5th Eur. Conf. on Antennas and Propag.*, Rome, Italy, Apr. 11–15 2011, pp. 812–815.

[8] H. Shi and A. Tennant, "Secure physical-layer communication based on directly modulated antenna arrays," in *Proc. Antennas and Propag. Conf. (LAPC)*, Loughborough, UK, Nov. 12–13 2012, pp. 1–4.

[9] A. Narbudowicz, D. Heberling and M. J. Ammann, "Low-cost directional modulation for small wireless sensor nodes," in *Proc. 10th Eur. Conf. on Antennas and Propag.*, Davos, Switzerland, Apr. 10–15 2016, pp. 1-3.

[10] Y. Ding and V. Fusco, "Vector representation of directional modulation transmitters," in *Proc. 8th Eur. Conf. on Antennas and Propag.*, Hague, Netherlands, Apr. 6–11 2014, pp. 367–371.

[11] Y. Ding and V. Fusco, "Directional modulation transmitter synthesis using particle swarm optimization," in *Proc. Antennas and Propag. Conf. (LAPC)*, Loughborough, UK, Nov. 11–12 2013, pp. 500–503.

[12] Y. Ding and V. Fusco, "BER driven synthesis for directional modulation secured wireless communication," *Int. J. Microw. Wireless Technol.*, vol. 6, no. 2, pp. 139–149, Apr. 2014.

[13] Y. Ding and V. Fusco, "Directional modulation transmitter radiation pattern considerations," *IET Microw., Antennas Propag.*, vol. 7, no. 15, pp. 1201–1206, Dec. 2013.

[14] Y. Ding and V. Fusco, "Constraining directional modulation transmitter radiation patterns," *IET Microw., Antennas Propag.*, vol. 8, no. 15, pp. 1408–1415, Dec. 2014.

[15] Y. Ding and V. Fusco, "Synthesis of directional modulation arrays for circular polarization transmission," in *Proc. 17th Research Colloquium on Commun. Radio Sci. into the 21st Century*, May, 2014.

[16] Y. Ding and V. Fusco, "A far-field pattern separation approach for the synthesis of directional modulation transmitter arrays," in *Proc. XXXIst URSI General Assembly and Scientific Symposium (GASS)*, Beijing, China, Aug. 16–23 2014.

[17] Y. Ding and V. Fusco, "Directional modulation far-field pattern separation synthesis approach," *IET Microw., Antennas Propag.*, vol. 9, no. 1, pp. 41–48, Jan. 2015.

[18] J. Hu, F. Shu and J. Li, "Robust synthesis method for secure directional modulation with imperfect direction angle," *IEEE Commun. Lett.*, vol. 20, no. 6, pp. 1084–1087, Jun. 2016.

[19] Y. Ding and V. Fusco, "Establishing metrics for assessing the performance of directional modulation systems," *IEEE Trans. Antennas Propag.*, vol. 62, no. 5, pp. 2745–2755, Feb. 2014.

[20] Y. Ding and V. Fusco, "Experiment of digital directional modulation transmitters," *Forum for Electromagn. Research Methods and Application Technol. (FERMAT)*, vol. 11, Sept.–Oct., 2015.

[21] Y. Ding and V. Fusco, "Orthogonal vector approach for synthesis of multi-beam directional modulation transmitters," *IEEE Antennas Wireless Propag. Lett.*, vol. 14, pp. 1330–1333, Feb. 2015.

[22] Y. Ding and V. Fusco, "MIMO-inspired synthesis of directional modulation systems," *IEEE Antennas Wireless Propag. Lett.*, vol. 15, pp. 580–584, 2016.

[23] H. Shi and A. Tennant, "Simultaneous, multi-channel, spatially directive data transmission using direct antenna modulation," *IEEE Trans. Antennas Propag.*, vol. 62, no. 1, pp. 403-410, Jan. 2014.

[24] Y. Ding and V. Fusco, "Improved physical layer secure wireless communications using a directional modulation enhanced retrodirective array," in *Proc. XXXIst URSI General Assembly and Scientific Symposium (GASS)*, Beijing, China, Aug. 16–23 2014.

[25] Y. Ding and V. Fusco, "Directional modulation-enhanced retrodirective array," *Electron. Lett.*, vol. 51, no. 1, pp. 118–120, Jan. 2015.

[26] Y. Ding and V. Fusco, "A review of directional modulation technology," *Int. J. Microw. Wireless Technol.*, to be published.

[27] Y. Ding and V. Fusco, "Development in directional modulation technology," *Forum for Electromagn. Research Methods and Application Technol. (FERMAT)*, vol. 13, Jan.–Feb. 2016.

[28] N. Valliappan, A. Lozano, and R. W. Heath, "Antenna subset modulation for secure millimeter-wave wireless communication," *IEEE Trans. Commun.*, vol. 61, pp. 3231–3245, Aug. 2013.

[29] N. N. Alotaibi and K. A. Hamdi, "Switched phased-array transmission architecture for secure millimeter-wave wireless communication," *IEEE Trans. Commun.*, vol. 64, no. 3, pp. 1303–1312, Mar. 2016.

[30] Q. Zhu, S. Yang, R. Yao, and Z. Nie, "A directional modulation technique for secure communication based on 4D antenna arrays," in *Proc. 7th Eur. Conf. on Antennas and Propag.*, Gothenburg, Sweden, Apr. 8–12 2013, pp. 125–127.

[31] Q. Zhu, S. Yang, R. Yao, and Z. Nie, "Directional modulation based on 4-D antenna arrays," *IEEE Trans. Antennas Propag.*, vol. 62, no. 2, pp. 621–628, Feb. 2014.

[32] Y. Zhang, Y. Ding, and V. Fusco, "Sidelobe modulation scrambling transmitter using Fourier Rotman lens," *IEEE Trans. Antennas Propag.*, vol. 61, no. 7, pp. 3900-3904, Jul. 2013.

[33] Y. Ding and V. Fusco, "Sidelobe manipulation using Butler matrix for 60 GHz physical layer secure wireless communication," in *Proc. Antennas and Propag. Conf. (LAPC)*, Loughborough, UK, Nov. 11–12 2013, pp. 61-65.

[34] Y. Ding, Y. Zhang, and V. Fusco, "Fourier Rotman lens enabled directional modulation transmitter." *Int. J. Antennas Propag.*, vol. 2015, Article ID 285986, 13 pages, 2015.

[35] L. Chen, Y. Guo, X. Shi, and T. Zhang, "Overview on the phase conjugation techniques of the retrodirective array," *Int. J. Antennas Propag.*, vol. 2010, pp. 1–10, Apr. 2010, article ID 564357.

[36] V. Fusco and N. Buchanan, "Developments in retrodirective array technology," *IET Microw., Antennas Propag.*, vol. 7, no. 2, pp. 131–140, May 2013.

[37] T. Hong, M. Z. Song, and Y. Liu, "Dual-beam directional modulation technique for physical-layer secure communication," *IEEE Antennas Wireless Propag. Lett.*, vol. 10, pp. 1417–1420, Dec. 2011.

[38] T. F. Chun, A. Zamora, J. Bao, R. T. Iwami, and W. A. Shiroma, "An interleaved, interelement phase-detecting/phase-shifting retrodirective antenna array for interference reduction," *IEEE Antennas Wireless Propag. Lett.*, vol. 10, pp. 919–922, Sept. 2011.

[39] V. Fusco, Y. Ding, and N. Buchanan, "Spectral signature secured retrodirective array," submitted for publication.

[40] N. Buchanan and V. Fusco, "Modulation insensitive PLL for tracking antenna applications," *Microw. Opt. Technol. Lett.*, vol. 57, no. 6, pp. 1286–1289, Jun. 2015.

[41] V. F. Fusco, "Response of retrodirective array in the presence of multiple spatially separated sources," *IEEE Trans. Antennas Propag.*, vol. 54, no. 4, pp. 1352–1354, Apr. 2006.

[42] T. F. Chun, M. K. Watanabe, A. Zamora, R. T. Iwami, J. M. Akagi, and W. A. Shiroma, "Analysis of phase-conjugating arrays in multiple-interrogator environments," in *Proc. IEEE Int. Conf. Wireless Inf. Technol. Syst.*, Honolulu, HI, Aug. 2010, pp. 1–4.

[43] V. Fusco and N. Buchanan, "Retrodirective antenna spatial data protection," *IEEE Antennas Wireless Propag. Lett.*, vol.8, pp.490–493, Apr. 2009.

[44] "WinProp release V 11.06," AWE Communications. Available at http://www.awe-communications.com, accessed August 2015.